

Exciton-exciton annihilation in a disordered molecular system by direct and multistep Förster transfer

Franziska Fennel and Stefan Lochbrunner*

Institut für Physik, Universität Rostock, Albert-Einstein-Str. 23, 18059 Rostock, Germany

(Received 6 January 2015; revised manuscript received 28 July 2015; published 13 October 2015)

Exciton annihilation dynamics in a disordered organic model system is investigated by ultrafast absorption spectroscopy. We show that the temporal evolution of the exciton density can be quantitatively understood by applying Förster energy transfer theory to describe the diffusion of the excitons as well as the annihilation step itself. To this end, previous formulations of Förster theory are extended to account for the inhomogeneous distribution of the S_0 - S_1 transition energies resulting in an effective exciton diffusion constant. Two annihilation pathways are considered, the direct transfer of an exciton between two excited molecules and diffusive motion by multiple transfer steps towards a second exciton preceding the annihilation event. One pathway can be emphasized with respect to the other by tuning the exciton diffusion constant via the chromophore concentration. The investigated system allows one to extract all relevant parameters for the description and provides in this way a proof that the annihilation dynamics can be entirely understood and modeled by Förster energy transfer.

DOI: [10.1103/PhysRevB.92.140301](https://doi.org/10.1103/PhysRevB.92.140301)

PACS number(s): 78.66.Qn, 71.35.-y, 78.47.D-, 78.55.Kz

Sufficiently large migration distances of Frenkel excitons in organic polymers and molecular systems are of high relevance for applications such as artificial light harvesting systems, molecular nanostructures, and organic light emitting diodes [1–3]. The exciton mobility is a key parameter to judge the suitability of a material for such applications [4]. At high excitation densities, high exciton mobilities or a combination of both, exciton-exciton annihilation (EEA), can occur [5,6], which is the deactivation of excitons by the fusion of two of them. On one hand, EEA is a valuable tool to characterize the mobility of excitons [7]. On the other hand, it is essential for understanding the exciton dynamics in organic materials such as polymers [8], nanostructures such as carbon nanotubes [9], bichromophoric molecules [10], and light responding functional molecules such as molecular optical switches [11].

In order to understand the annihilation dynamics, two basic exciton transfer steps, i.e., the transfer from an excited to an unexcited molecule and the transfer of an exciton between two excited molecules, have to be considered. In the case of weakly coupled systems, as will be examined here, the exciton transfer is incoherent and thus the transfer rates can be determined by means of Förster theory (for limits of the Förster theory, see Ref. [12]). In the case of strongly coupled systems, more sophisticated models have to be applied, which e.g., treat the coupling between the molecules explicitly [13] and incorporate two exciton states in the description of annihilation events [14].

The exciton transfer rate between an excited donor and an acceptor in the ground state is given by the spectral overlap between the exciton emission and the ground state absorption (GSA) [see Fig. 1(a)]. Several of such transfer steps lead to a continuous exciton migration which is described in the following by a diffusion approach. The energetic disorder present in most organic systems has a strong impact on the

exciton diffusion as the rates of the individual steps depend sensitively on the transition energies of the two partners, as it was shown, e.g., for nanocrystals [15]. Therefore, a proper description of the exciton diffusion in disordered systems has to take the energetic disorder into account. In this Rapid Communication an ensemble average of the individual energy transfer steps is applied which enables to calculate the exciton diffusion constant in energetically disordered systems.

The exciton transfer between two excited molecules, called exciton fusion, is also described via the Förster formalism with a spectral overlap between the exciton emission and the absorption of the exciton state to higher electronic S_n states (ESA) [10] [see Fig. 1(b)]. The fusion of two excitons is the decisive process of exciton annihilation, as the highly excited state generated by the fusion event is short lived and relaxes quickly to the S_1 state, and thereby quenching efficiently one exciton.

In this Rapid Communication we examined the annihilation dynamics for a disordered model system, featuring dye molecules in a polymer matrix with ultrafast pump probe spectroscopy. The pump pulse generates a defined number of excitons and the temporal evolution of this exciton density is measured with the time delayed probe pulse. The temporal evolution of the exciton density $n(t)$ is given by [16,17]

$$\frac{dn(r,t)}{dt} = -k_s n(r,t) - \frac{1}{2} k_Q(t) n^2(r,t), \quad (1)$$

where k_s is the intramolecular decay rate and $k_Q(t)$ the time-dependent annihilation rate per exciton. The factor of one half in the second term results from the fact that one exciton survives an annihilation event. The annihilation rate k_Q is given by [16,17]

$$k_Q(t) = 4\pi D \left[\bar{a} + \frac{\bar{a}^2}{\sqrt{\pi D t}} \right] \quad \text{with} \quad \bar{a} = 0.676 \sqrt[4]{\frac{R_{ESA}^6}{D \tau_{rad}}}, \quad (2)$$

where D is the diffusion constant of the excitons, \bar{a} the typical distance between two excitons for fusion, and R_{ESA}

*Stefan.Lochbrunner@uni-rostock.de

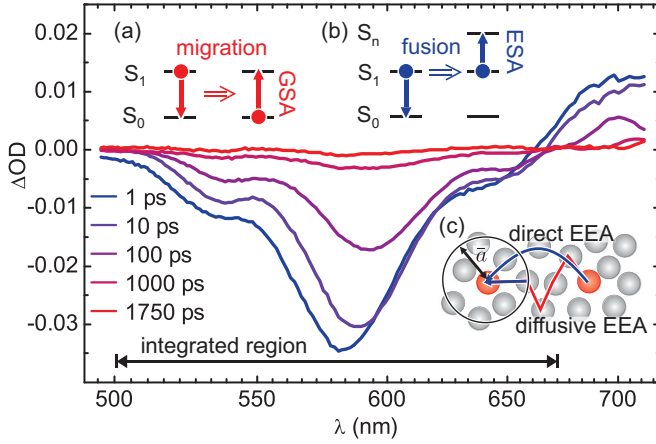


FIG. 1. (Color) Transient absorption spectra for a dye concentration of 100 mM and an initial excitation density of $7.13 \times 10^{-3} \text{ nm}^{-3}$. The dominant band results from the overlap of the ground state bleach and stimulated emission. (a) and (b) show the two different exciton transfer mechanisms, and (c) the contributing annihilation channels (for details see text).

the Förster radius associated with the exciton fusion. The first term of the annihilation rate in Eq. (2) describes the approach of two excitons via diffusion and subsequent fusion—this contribution is called diffusive EEA. The second part arises from direct exciton fusion without initial migration. The time dependence of $t^{-1/2}$ is known from Förster theory [18] and results as the exciton pairs in close proximity annihilate first, while with time the average distance between the surviving excitons increases, leading to a decrease of direct EEA events. Both annihilation channels, direct and diffusive EEA, are schematically depicted in Fig. 1(c).

Using Eq. (2), the rate Eq. (1) can be solved analytically, leading to

$$n(t) = \frac{e^{-t/\tau_s}}{\frac{1}{n_0} + \underbrace{\bar{a}^2 \sqrt{8D\tau_s\pi} \operatorname{erf}\left(\frac{t}{\tau_s}\right)^{\frac{1}{2}}}_{\text{diffusive EEA}} + \underbrace{4\pi D\bar{a}\tau_s(1 - e^{-t/\tau_s})}_{\text{direct EEA}}}. \quad (3)$$

Both annihilation channels contribute to the denominator, leading to a faster decay of the excitons. The different time dependencies enable one to discriminate between diffusion and fusion, and thus the diffusion constant D and the Förster radius for exciton fusion R_{ESA} can be determined simultaneously.

The exciton diffusion constant D can be calculated by [19]

$$D = \eta \left(\frac{4\pi c}{3} \right)^{\frac{4}{3}} \frac{R_0^6}{\tau_{\text{rad}}}, \quad (4)$$

where c is the concentration of the dye molecules, R_0 the Förster radius for the transfer between an excited molecule and a molecule in the ground state, and η a constant prefactor, here 0.428 [19] for an orientational disordered system. The radiative lifetime τ_{rad} is obtained by the Strickler-Berg relation [20]. The intramolecular lifetime of the exciton $\tau_s = 1/k_s$ is obtained from the quantum yield $\Phi = \frac{\tau_s}{\tau_{\text{rad}}}$. The Förster radii R_0 and

R_{ESA} are calculated by [21,22]

$$R_{0,\text{ESA}} = (C \times J_{0,\text{ESA}})^{\frac{1}{6}},$$

$$J_{0,\text{ESA}} = \int_{-\infty}^{\infty} \frac{\varepsilon_{0,\text{ESA}}(\nu) F(\nu)}{\nu^4} d\nu, \quad (5)$$

$$C = \frac{9f^2 \ln 10}{128\pi^5 N_A n^4},$$

where f^2 is an orientation factor obtained by averaging over different transition dipole orientations and amounts to 0.476 for a solid host [23]. N_A is Avogadro's constant, n the refractive index, and J the spectral overlap integral in which the molar extinction coefficient ε of the acceptor and the fluorescence spectrum F of the donor are integrated along the wave number ν axis. In the case of a material with an inhomogeneous distribution of site energies, as in the present situation [24], the exciton diffusion constant is significantly smaller than the direct calculations of the overlap integral J from the spectral signatures suggest, since Eq. (5) neglects inhomogeneous broadening. To overcome this problem, inhomogeneous broadening is accounted for by decomposing the spectral width in a homogeneous and an inhomogeneous contribution. The spectral overlap between two partners is then dependent on the homogeneous width and their site energies. As the diffusion constant is proportional to J , the ensemble average of J is performed. Thereto, the overlap between two partners is weighted with the density of acceptor states and the population density of the donors. Although the pump pulse generates an exciton distribution proportional to the total inhomogeneous distribution, the donors are considered to be in thermal equilibrium. This assumption is valid for a fast energetic relaxation, which holds in the present situation due to the mobility of the excitons. In the case of slow exciton transfer this assumption fails as energetic relaxation takes place on time scales comparable to annihilation, leading to a time-dependent diffusion constant [25].

By integrating over the donor and acceptor energies one obtains [26]

$$R_{0,\text{mean}}^6 = C \frac{\sqrt{\pi} \varepsilon_{\text{max}} F_{\text{max}} \sigma_t}{\nu_0^4} e^{-\frac{(s - \frac{\sigma_t^2}{4\sigma_i^2})^2}{4\sigma_i^2}}. \quad (6)$$

Here, ε_{max} is the molar extinction coefficient at the absorption maximum and F_{max} the maximum of the fluorescence spectrum, where the area underneath the spectrum is normalized to one. σ_t and σ_i are the total and the inhomogeneous widths of the Gaussians representing the spectra and S is the Stokes shift. Equation (6) allows one, in combination with Eq. (4), to calculate realistic values for the diffusion constant in the presence of energetic disorder, extending previous approaches based on Förster theory which neglected energetic disorder [19].

The annihilation study was carried out with an organic guest-host model system consisting of 1,6,7,12-tetraphenoxy-N,N0-bis(2,6-di-isopropylphenyl)-3,4,9,10-perylenedicarboximide (Perylene Red) dye molecules (supplied by BFI Optilas) as active sites dispersed in a polymer host of poly(methyl methacrylate) (PMMA). This combination enables relatively high dye concentrations

without aggregation. The samples were prepared by spin coating. Their thicknesses were in the range of 1–10 μm (for determination of the film thickness, see Ref. [27]) to ensure an optical density below 0.2 at the excitation wavelength. Samples with dye concentrations of 10, 34, 55, and 100 mM exhibiting different exciton mobilities were investigated. Higher dye concentrations were not used since the diffusion constants then no longer scale with the characteristic behavior of $c^{4/3}$ [27]. This breakdown of the diffusive motion is a common feature also observed for other dyes at high molecular concentrations, as it was recently shown for subphthalocyanine chloride [28]. Furthermore, the limit of Förster theory is approached, since the dipole approximation is invalid for close packing and the shielding effect of PMMA can no longer be described with a continuum approach which yields the factor n^4 in Eq. (5) [12].

Transient absorption measurements were performed with a setup similar to Refs. [29,30]. The samples were excited at 530 nm by 40 fs long laser pulses from a noncollinear optical-parametric amplifier, and the transient absorption was recorded with a white light continuum. Details on the setup and the determination of the exciton density are given in the Supplemental Material (SM) [26].

For the annihilation study, a signal proportional to the exciton density, free of signatures caused by energetic relaxation or internal vibrational redistribution, is needed. To this end, the change of optical density was integrated over the spectral range of 500–670 nm covering most of the ground state bleach (GSB) and the stimulated emission (SE) (see Fig. 1). The resulting signal is scaled to the initial exciton density and reflects directly the time-dependent exciton density.

The temporal evolution of the exciton density in samples with dye concentrations of 10 mM [Fig. 2(a)] and 55 mM [Fig. 2(b)] is depicted in Fig. 2. The decay of the excitons accelerates with exciton density (see the insets of Fig. 2) and with concentration [see Figs. 2(a) and 2(b)]. The acceleration of the EEA with the dye concentration is caused by higher absolute exciton densities and the increasing diffusion constant ($D \propto c^{4/3}$). A direct comparison of curves (see SM [26]) with the same initial exciton density but different dye concentrations shows that the exciton density decays faster for high dye concentrations, i.e., high diffusion constants. This proves that exciton diffusion contributes to annihilation, at least at high concentrations.

Equation (3) is fitted for a specific dye concentration simultaneously to five data curves with different known initial exciton densities by varying D and R_{ESA} . The lifetime τ_s of Perylene Red in PMMA is given by the radiative lifetime $\tau_{\text{rad}} = 6.4$ ns [24] and the quantum yield [27] (see Table I). Good agreement between the measured and modeled temporal evolution of the exciton density is achieved (see the colored curves in Fig. 2). The obtained values for R_{ESA} and D are listed in Table I.

The diffusion constant D scales roughly with $c^{4/3}$, as it is expected from Eq. (4). From all experiments comparable excited state Förster radii R_{ESA} in the range between 5.1 and 5.7 nm were obtained, indicating that the applied EEA model [Eq. (3)] is consistent with the measured data.

The diffusion constant D of the exciton motion can be compared to experimental diffusion constants obtained by the

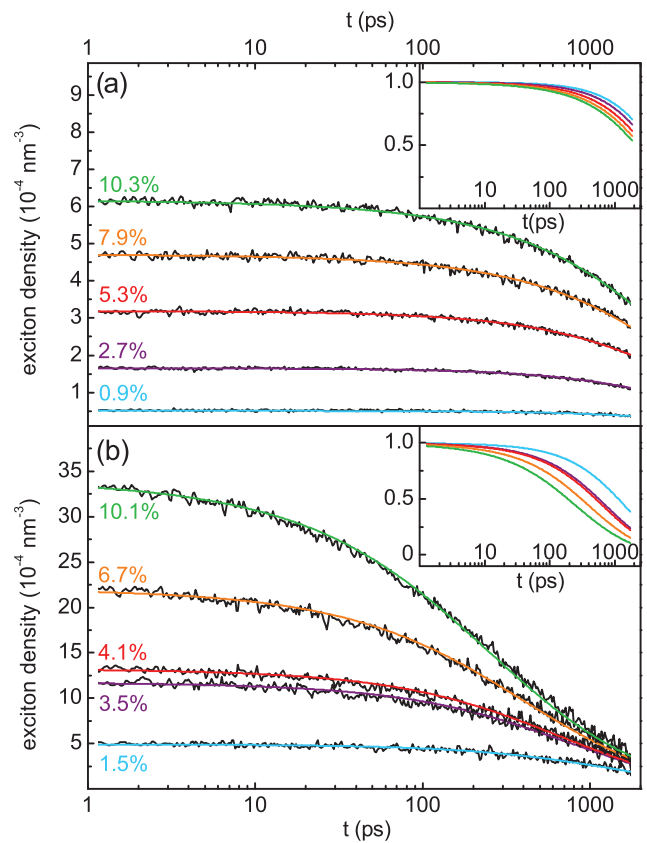


FIG. 2. (Color) Decay of the exciton population for (a) 10 mM and (b) 55 mM of Perylene Red in PMMA for different initial exciton densities (black curves). The exciton density is given in percent of the chromophore concentration. Colored curves are fits according to Eq. (3). The insets show the exciton dynamics for different initial excitation densities normalized to one.

bulk quenching method in Ref. [27]. Those were measured at slightly different concentrations, and after correcting this with a scaling of $c^{4/3}$, the values listed in Table I, column 5 are obtained. The values extracted with the two different experimental methods match very well, taking into account the uncertainties in the experimental determination of concentrations and lifetimes.

TABLE I. The first four columns list the parameters used to fit Eq. (3) to the time dependent exciton density for the different concentrations, thereby only D and R_{ESA} were adjusted. Column five and six are the values of the diffusion constant according to [27] and calculated by Eq. (4) with the parameters (for details see SI [26]) $\varepsilon_{\text{max}} = 48\,000 \text{ M}^{-1} \text{ cm}^{-1}$, $F_{\text{max}} = 5.375 \times 10^{-4} \text{ cm}$, $S = 721 \text{ cm}^{-1}$, $\nu_0 = 16\,990 \text{ cm}^{-1}$, $\sigma_i = 260 \text{ cm}^{-1}$, $\sigma_f = 470 \text{ cm}^{-1}$, $n = 1.49$, $k_B T = 200 \text{ cm}^{-1}$ taken from [24]. Column seven is the excited state Förster radius calculated by Eq. (5). Förster radii are given in nm and diffusion constants in nm^2/ns .

1.	2.	3.	4.	5.	6.	7.
c (mM)	Φ [27]	D	R_{ESA}	D [27]	D [Eq. (4)]	R_{ESA} [Eq. (5)]
10	0.99	5	5.1	2.2	3	5.9
34	0.90	9	5.7	11	16	5.8
55	0.78	21	5.7	22	30	5.9
100	0.52	36	5.4	48	66	5.9

To test the predictive power of the Förster model, the diffusion constant was calculated by Eq. (4) from the spectral properties of the samples and compared to the experimental values. With the spectral parameters given in the caption of Table I, a value of $R_{0,\text{mean}} = 4.28$ nm is obtained via Eq. (6), resulting in the calculated diffusion constants listed in Table I, column 6.

The computed diffusion constants are realistic although slightly larger than the ones extracted by fitting the annihilation model. Several parameters used for the calculation, such as the linewidths, the S_1 lifetime, and the concentrations, are associated with significant uncertainties. The accumulation of the individual errors results in a total error of 15% (for details, see SM [26]). The major contribution is given by the uncertainty of the inhomogeneous broadening σ_i (accuracy of ± 20 cm $^{-1}$ [27]), since the overlap integral depends exponentially on σ_i . Additionally, there is some ambiguity in the prefactor η in Eq. (4) and values between 0.32 and 0.56 are reported, depending on the calculation method and the sample structure [16,21,31–33]. At high concentrations one also expects small deviations from the dipole approximation, and treating the molecules as point particles might no longer be appropriate. Taking all this into account, the observed deviations between fitted and calculated diffusion constants are reasonable.

Furthermore, we estimated R_{ESA} from the overlap integral of the fluorescence with the ESA extinction. The ESA is determined from the transient spectra by subtracting GSB and SE [34]. The reconstruction of the ESA is associated with large uncertainties with respect to the exact shape. In particular, artificial wiggles are found. They result most probably from spectral shifts of the ESA and GSB due to vibrational redistribution which are not taken into account since information about them is lacking. For a detailed discussion of the ESA, see SM [26] and compare Refs. [10,35–37]. From the resulting overlap integral the excited state Förster radius can be calculated by Eq. (5), leading to a radius in the range of 5.8–5.9 nm (see Table I, column 7). The value is of the same order as the one extracted by the annihilation model, thereby supporting the correctness of the EEA model.

The comparison between calculated and experimentally determined diffusion constants and excited state Förster radii demonstrates not only that the dynamics of EEA can be understood in terms of Förster energy transfer events, but that our approach provides a route for a realistic simulation of the exciton diffusion and the EEA.

For a deeper understanding of the relevant annihilation channels, the impact of the two different channels, direct and diffusive EEA, was evaluated. For the concentration of 10 mM, direct EEA dominates the annihilation as the respective term in Eq. (3) is for all times larger than the diffusion EEA term. With increasing dye concentration the diffusive channel gains relevance and dominates the annihilation at high concentration. Therefore, by varying the concentration, the driving annihilation process can be altered.

Whether the data can be described by only one of the processes is checked by either setting direct EEA or diffusive EEA to zero, while the relevant parameter of the operating

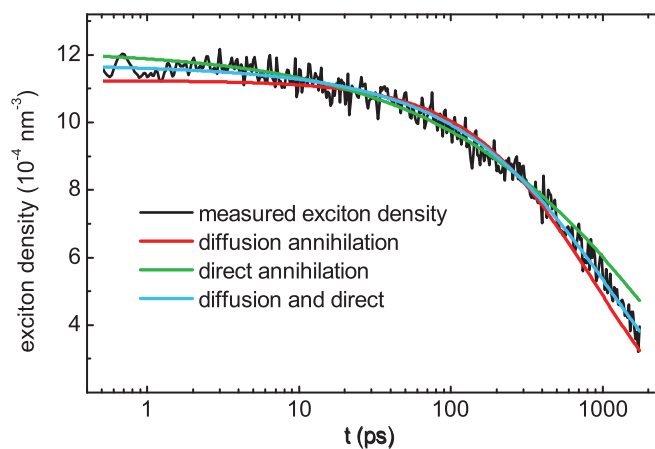


FIG. 3. (Color) Temporal behavior of the exciton density for a sample with a Perylene Red concentration of 34 mM, and an initial exciton density of $11.6 \times 10^{-4} \text{ nm}^{-3}$. The data are compared to fits of Eq. (3), taking either only diffusive EEA or only direct EEA or both processes into account.

channel, i.e., either D or R_{ESA} , is optimized to obtain a minimal deviation between the fit and measured data. For all concentrations considered here, it was impossible to achieve satisfactory agreement between the two, as it is shown in Fig. 3 for a dye concentration of 34 mM. Concluding, both channels make a relevant contribution.

In summary, a model resting solely on Förster energy transfer is presented that is able to describe EEA in an inhomogeneous organic guest-host system quantitatively. It takes two channels into account, direct and diffusive EEA. Both annihilation channels are in a delicate balance and already rather small changes in the sample properties, e.g., concentration, can change the impact of either channel. The energetic inhomogeneity is accounted for by a mean overlap integral, resulting in an ensemble averaged diffusion constant for an energetically disordered system in its thermal equilibrium. It is shown that the two key parameters extracted from the annihilation model, the diffusion constant D and the excited state Förster radius R_{ESA} , are consistent with the spectral properties of the system within the framework of Förster theory. In particular, it is possible to predict the exciton diffusion constant in energetically disordered systems with a reasonable accuracy using Eqs. (4) and (6). We are confident that this description can also be applied to many other systems, such as polymers [8], molecular systems [38], and nanostructures [39]. The present work provides extended prospects for EEA studies by a quantitative description of the basic processes in inhomogeneous systems.

We are grateful to the Deutsche Forschungsgemeinschaft for financial support of this work within the SFB 652 “Strong correlation and collective effects in radiation fields: Coulomb systems, clusters and particles” and the associated graduate school. F.F. is thankful to the Stiftung der Deutschen Wirtschaft for support via a graduate fellowship. We thank Oliver Kühn and Sergei Ivanov for valuable discussions.

- [1] K.-T. Wong and D. M. Bassani, *NPG Asia Mater.* **6**, e116 (2014).
- [2] J.-S. Huang, T. Goh, X. Li, M. Y. Sfeir, E. A. Bielinski, S. Tomasulo, M. L. Lee, N. Hazari, and A. D. Taylor, *Nat. Photonics* **7**, 480 (2013).
- [3] G. D. Scholes, G. R. Fleming, A. Olaya-Castro, and R. van Grondelle, *Nat. Chem.* **3**, 763 (2011).
- [4] P. Heremans, D. Cheyns, and B. P. Rand, *Acc. Chem. Res.* **42**, 1740 (2009).
- [5] G. Trinkunas, J. L. Herek, T. Polívka, V. Sundström, and T. Pullerits, *Phys. Rev. Lett.* **86**, 4167 (2001).
- [6] I. G. Scheblykin, A. Yartsev, T. Pullerits, V. Gulbinas, and V. Sundström, *J. Phys. Chem. B* **111**, 6303 (2007).
- [7] J. D. A. Lin, O. V. Mikhnenko, J. Chen, Z. Masri, A. Ruseckas, A. Mikhailovsky, R. P. Raab, J. Liu, P. W. M. Blom, M. A. Loi, C. J. Garcia-Cervera, I. D. W. Samuel, and T.-Q. Nguyen, *Mater. Horiz.* **1**, 280 (2014).
- [8] F. Steiner, J. Vogelsang, and J. M. Lupton, *Phys. Rev. Lett.* **112**, 137402 (2014).
- [9] Y. Z. Ma, L. Valkunas, S. L. Dexheimer, S. M. Bachilo, and G. R. Fleming, *Phys. Rev. Lett.* **94**, 157402 (2005).
- [10] J. Hofkens, M. Cotlet, T. Vosch, P. Tinnefeld, K. Weston, C. Ego, A. Grimsdale, K. Müllen, D. Beljonne, J. L. Bredas, S. Jordens, G. Schweitzer, M. Sauer, and F. De Schryver, *Proc. Natl. Acad. Sci. U.S.A.* **100**, 13146 (2003).
- [11] B. Fückel, G. Hinze, F. Nolde, K. Müllen, and T. Basché, *Phys. Rev. Lett.* **103**, 103003 (2009).
- [12] D. Beljonne, C. Curutchet, G. D. Scholes, and R. J. Silbey, *J. Phys. Chem. B* **113**, 6583 (2009).
- [13] P.-A. Plötz, T. Niehaus, and O. Kühn, *J. Chem. Phys.* **140**, 174101 (2014).
- [14] V. May, *J. Chem. Phys.* **140**, 054103 (2014).
- [15] K. Becker, J. M. Lupton, J. Müller, A. L. Rogach, D. V. Talapin, H. Weller, and J. Feldmann, *Nat. Mater.* **5**, 777 (2006).
- [16] S. Jang, K. J. Shin, and S. Lee, *J. Chem. Phys.* **102**, 815 (1995).
- [17] U. Gösele, M. Hauser, U. K. A. Klein, and R. Frey, *Chem. Phys. Lett.* **34**, 519 (1975).
- [18] T. Förster, *Z. Naturforsch.* **4a**, 321 (1949).
- [19] C. R. Gochanour, H. C. Andersen, and M. D. Fayer, *J. Chem. Phys.* **70**, 4254 (1979).
- [20] S. J. Strickler and R. A. Berg, *J. Chem. Phys.* **37**, 814 (1962).
- [21] T. Förster, *Ann. Phys.* **437**, 55 (1948).
- [22] G. D. Scholes, *Annu. Rev. Phys. Chem.* **54**, 57 (2003).
- [23] J. R. Lakowicz, *Principles of Fluorescence Spectroscopy*, 3rd ed. (Springer, Berlin, 2006).
- [24] F. Fennel and S. Lochbrunner, *Phys. Rev. B* **85**, 094203 (2012).
- [25] S. M. King, D. Dai, C. Rothe, and A. P. Monkman, *Phys. Rev. B* **76**, 085204 (2007).
- [26] See Supplemental Material at <http://link.aps.org/supplemental/10.1103/PhysRevB.92.140301> for a detailed derivation of Eq. (6), and the determination of the excitation density. Furthermore, the SM contains additional measurements, and the error propagation for the diffusion constant.
- [27] F. Fennel and S. Lochbrunner, *Phys. Chem. Chem. Phys.* **13**, 3527 (2011).
- [28] S. M. Menke, W. A. Luhman, and R. J. Holmes, *Nat. Mater.* **12**, 152 (2013).
- [29] U. Megerle, I. Pugliesi, C. Schrieffer, C. F. Sailer, and E. Riedle, *Appl. Phys. B* **96**, 215 (2009).
- [30] H. Marciniak, X.-Q. Li, F. Würthner, and S. Lochbrunner, *J. Phys. Chem. A* **115**, 648 (2010).
- [31] S. W. Haan and R. Zwanzig, *J. Chem. Phys.* **68**, 1879 (1978).
- [32] R. F. Loring, H. C. Andersen, and M. D. Fayer, *J. Chem. Phys.* **80**, 5731 (1984).
- [33] C. J. Bardeen, *Annu. Rev. Phys. Chem.* **65**, 127 (2014).
- [34] A. V. Deshpande, A. Beidoun, A. Penzkofer, and G. Wagenblast, *Chem. Phys.* **142**, 123 (1990).
- [35] F. Würthner, *Chem. Commun.* **14**, 1564 (2004).
- [36] Z. Chen, U. Baumeister, C. Tschierske, and F. Würthner, *Chem. Eur. J.* **13**, 450 (2007).
- [37] J. Hofkens, T. Vosch, M. Maus, F. Köhn, M. Cotlet, T. Weil, A. Herrmann, K. Müllen, and F. C. De Schryver, *Chem. Phys. Lett.* **333**, 255 (2001).
- [38] C. G. Hübner, G. Zumofen, A. Renn, A. Herrmann, K. Müllen, and T. Basché, *Phys. Rev. Lett.* **91**, 093903 (2003).
- [39] G. M. Akselrod, J. R. Tischler, E. R. Young, D. G. Nocera, and V. Bulovic, *Phys. Rev. B* **82**, 113106 (2010).